Diatom and Diatomite: Different Focus on Natural Media to Material Science Path

Secou Sall[1], Vasiliki Papaefthimiou[1], Thierry Dintzer[1], Fabrice Vigneron[1], Eric Brendlé[2], Pierre Petit[3], Tom Ferte[4], Saliha Haddoum[5], Sana Labidi[1*], Corinne Petit[1]

[1]ICPEES, UMR-CNRS 7515, Strasbourg University, Strasbourg, France
[2]Adscientis, Wittelsheim, France
[3]ICS, CNRS UPR 22, Strasbourg, France
[4]IPCMS, UMR CNRS 7504, Strasbourg University, Strasbourg, France
[5]Ecole Nationale Polytechnique, El-Harrach, Algeria
Email: ssall@unistra.fr, papaefthymiou@unistra.fr, thierry.dintzer@unistra.fr, fabrice.vigneron@unistra.fr,
e.brendle@adscientis.com, pierre.petit@ics-cnrs.unistra.fr, tom.ferte@ipcms.unistra.fr, saliha.haddoum@g.enp.edu.dz,
*slabidi@unistra.fr, corinne.petit@unistra.fr

Abstract

Bio-silica issued from diatom, a microalgae, is attracted increasing attention in material science thanks to its peculiar nanoarchitecture and related properties with versatile applications. The present work is a deep analysis on morphological and chemical properties of bio-silica issued from fossil origin (diatomaceous earth) and living one (algal paste). An optimization in purification protocol was performed to obtain multiparous bio-silica from its raw media with keeping its original shape entirely. Multiple characterization methods as scanning electronic microscopy (SEM), infrared spectroscopy, x-ray diffraction (DRX), X-ray photoelectron spectroscopy (XPS), energy dispersive X-ray spectroscopy (EDX), nitrogen adsorption and inverse gas chromatography (IGC), were used to check the purification protocol efficiency as well as to gather accurate information on morphology and chemical composition of diatom material obtained in large amount.

Keywords

Diatom, Diatomite, Bio-Silica, Purification, Frustule

1. Introduction

Diatom is a microalgae belonging to phytoplankton family, living in seawater and water streams. Living diatoms is a major part of Earth's biomass and ecosystem since they consume from aqueous media more than 6.7 billion metric

tons of silicon [1] and about 10 billion metric tons of CO_2 (equivalent to all of the world's rainforests activity) [2], per year respectively. Behaving like plants, diatoms produce chemical energy from light through photosynthesis and have specific anatomy since they are cells surrounded by a "glassy" porous wall [3] [4] [5]. This wall, called frustule, is made of amorphous silica in central or penal asbox nanostructured with porous pattern able to protect living cell from outside aggression and enabling, in the same time, nutriment sourcing [6] [7]. Once the biological cell is dead, the silica shell sediments and accumulates through geological timescale to produce diatomite, also called diatomaceous earth or kieselguhr. Two different shapes for diatoms could be considered: centric diatoms with radial symmetry and pinnate ones with bilateral symmetry which are dominant. The frustule structure with a "petri dish" architecture is composed of upper (epithecium) and lower (hypothecium) overlapping valves with a girdle band surrounding [8]. Each valve acts as an intricate 3D sieve with hierarchical porous structure with superposed sieve layers. A layer could be considered as honeycomb-like structure composed of walls called ridges separating pores called areola. The largest pores plate is called foramen and plates with the finest and intermediate pores are called cribellum and cribrum referring to as sieve plates [6] [9] [10].

Thanks to its peculiar shapes and interesting properties, biogenic silica diatoms shell exhibits valuable potentiality thanks to its mixed nano and microstructure which explain thousands of publications in distinct fields like marine biology, materials science, nanotechnology, optics, electronics, medicine and agriculture [11] [12] [13]. In addition, 3D nanoporous patterns of diatom frustules make it a convenient shuttle to internalize and release molecules (e.g., therapeutic agents for medical purpose) [14] and ordered porosity distribution of diatom frustule bears a similarity with photonic crystal [15]. Instead, diatoms show master craftsmanship with unlimited potential uses in tremendous increase.

All these fascinating properties can be stressed once diatom or diatomite is out of impurities. Cleaning protocols of diatomaceous earth or diatom algae from impurities include often mineral acid attacks (H_2SO_4, HCl, HNO_3…) or oxidative steps enhancing Si-OH surface density for a better use further [16] [17] [18] [19]. These hydroxyls bonds (-OH) could be tuned through silanization strategies to bind variable active molecules like metal nanoparticles, metal oxide nanoparticles, antibodies, etc. [20]. Some authors as Zhang *et al.* [21] reported cleaning protocol for diatomite sample of Coscinodiscus Ehrenberg sp. in water without use of chemical reagents but no characterizations have been done subsequently to check absence of impurities. Frustules after cleaning process are considered as safe and biocompatible bio-sourced silica without residual cleaning reagents. In spite of the interesting chemical properties and peculiar 3D nanostructure going beyond human ability, diatoms shells were ignored for long time by scientific community and attracted its attention only in the last century. First, Morse *et al.* [22] were the first group to bring to light biogenic silica of di-

atoms use in nanotechnology in 1999. They confirm that controlled nanoarchitecture of diatom shell is highly ordered, exceeding human ability, and elaborated in environmentally benign route.

All the acquired knowledge about bio-silica issued from diatomite/diatom is growing step by step after the increasing interest on bio-sourced material. Nevertheless, a transition of this material from its raw natural media to nanotechnology needs further investigation to control final properties and to understand its peculiarities for a large batch and not only for few diatom units. Producing pure diatom frustules with preserving its original shape at scalable amount is the first step to increase the maturity level of this material and make it closer to the market. Technology Readiness Level (TRL) is a metric parameter proposed by NASA to assess the maturity level of innovative product (0 is the basic research level and 9 is the full scale deployment level) and TRL5 and TRL6 are attributed to diatom frustules based biosensors [23]. This proves that biogenic silica is near to full scale deployment. Bio-silica could be a key factor to development of several application fields like sensors, biomedical, catalysis, optic thanks to its availability with renewable resourcing avoiding limitation of synthetic silica reagents (inorganic and polymeric materials) [23]. Progressing from TRL6 to highest levels needs checking full-scale engineering first which means using highest amount of materials with the same properties at lab and pilot scale [24]. This level upgrading means producing scalable quantity of homogeneous samples in shape and composition of diatom frustules with deep and precise knowledge of their properties. One of the objectives of this work is to validate upgrading purification protocol of diatom algal pate.

Frustule properties are different of synthetic silica materials as aerosyl, SBA or quartz regarding porous morphology, surface reactivity, chemical composition and its biocompatibility. Even frustules are made mainly of silica, biogenesis phase could lead to incorporation of other chemical elements from growing media.

This work is aimed to give further and extensive knowledge about diatom/diatomite material through deep characterization done in comparison with synthetic silica in some cases. So, the aim of this study is to prove that substituting synthetic silica by bio-silica is largely benefit regarding better architectural morphology of frustules and lower ecological footprint.

Diatomite raw rock or diatomaceous earth (fossil) and algal paste (living) undergone purification protocols in order to obtain a bio-silica material with high purity average and conserved 3D porous pattern. The purification challenge is different according to used sources. In the case of diatomite, the frustule is totally and partially smashed and is extracted from mineral mine and contains mineral impurities indeed while organic cell was decomposed. Concerning algal paste, the challenge is different since the biological cell is still present inside frustule shell. So, the extraction and elimination of biological fragments matter form algal paste must be accomplished without damaging the frustule 3D pattern. This is not trivial for two reasons. Firstly, the quantity of organic matter is

important [25] and secondly, the glassy sieve of frustule architecture surrounding cell could block its leaching and/or could be smashed. Concerning algal paste, the purification protocol must be optimized not only to enhance diatom frustules purity state, but also to obtain entire frustule as much as possible. This last target is with major importance because we want to obtain totally/mostly entire and pure frustules to take advantages of its original 3D structure entirely, which is not usually checked in literature. The present work proposes a scalable purification protocol to obtain large amount of pure frustules with entire 3D pattern to take advantage of its nanoarchitecture for the previous detailed applications.

2. Materials and Methods

2.1. Materials

The diatomaceous frustules observed in this work were obtained from two different sources: diatomite, the fossil rock and diatom living source. The fossil residues of diatom shells were collected from Sig mine, Mascara, at western cost of Algeria [26]. This mine consists of marine sediments of Late Miocene and Quaternary formations. Marine sediments of Late Miocene are founded on 4 levels: marls, diatomite or kieselguhr, siltstone and limestone. The diatomite layers contain centric *coscinosdiscus lineatus nitudus* as the major strain *according to Hadjadj Aoul O.* [26] and *Vanden Broeck J.* [27]. Diatom unspoilt source is a marine microalgae concentrated called "algal paste" specie-specified of *Thalassiosira weissflogii sp.* and purchased from Planktovie. For characterization with inverse gas chromatography, molecular probes (chloroform, benzene, tetrahydrofuran and diethyl ether) and ultra-pure silica gel were purchased from Merck with ≥99.9% purity.

2.2. Analytical Methods

Elemental mapping was carried out by energy dispersive X-ray spectroscopy (EDX) using a 6700F scanning electron microscope (cold FEG) from JEOL Company at an accelerating voltage of 15 kV and silicon drift detector (SDD) with a sensor size of 100 mm^2. The sample was covered with carbon layer of 20 nm thickness and deposited on a C-Al double tape on a Cu-Zn sample holder. The inverse gas chromatography (IGC) experiments were conducted by using a HRGC Mega 2 series (CE Instruments, UK) gas chromatograph with two channels. Helium 99.996% was used as the carrier gas and methane 99.995% was employed for the dead volume determination. The retention times of solute molecules and methane were determined using a flame ionization detector (FID). All experiments were undertaken in similar ambient conditions: at 20°C temperature and 1.013 atm pressure. Carrier gas flow rates of 10 sccm were employed in the experiments. Empty stainless columns (200 and 50 mm long with an I.D. of 2 mm) were filled with the solid sample by gentle vibration. Column ends were plugged with glass wool. Prior to experiments, the columns were preconditioned

(in situ) at 473K overnight. Dispersive surface energy, was determined by homologous series of n-alkanes (n-pentane, n-hexane, n-heptane, n-octane, n-decane and n-nonane) and acidity/basicity equilibrium constant (K_A-K_D) were accessed by polar probes injections (chloroforme, benzene, tetrahydrofuran and diethyl ether). γ_s^D, K_A and K_B were calculated using Nucleus (version 1.2.2, Adscientis) and SolID (version 3.2.1, Adscientis) softwares for experimental injections and calculation respectively. **N$_2$ adsorption-desorption** measurements were carried out on a Micromeritics ASAP 2020 instrument at the liquid N_2 temperature (77 K) and relative pressures between 0.01 and 0.98 P/P^0. Each sample was outgassed at 423 K under ultrahigh vacuum (10^{-6} Torr) for 12 h before the analysis in order to desorb moisture and adsorbed volatile species. Scanning electron microscopy **(SEM)** was carried out using a Hitachi SU8010 in ICS institute. Additional SEM analysis for diatom material has been done in ICPEES institute by Zeiss 2600F with a resolution of 5 nm. Samples were deposited onto a double-face graphite tape in order to avoid charging effects during the measurements. X-ray photoelectron spectroscopy **(XPS)** measurements were performed using an ultrahigh vacuum MULTILAB 2000 (THERMO VG) spectrometer equipped with a RESOLVE 120 MCD5 hemi-spherical electron analyzer. The Al Ka line (Al Ka, $h\nu$ 1/4 1486.6 eV) of a dual anode X-ray source was used as the incident radiation. Survey and high-resolution spectra were recorded in constant pass energy mode (90 and 22 eV, respectively). Binding energies were calibrated by referring to the C 1s peak at 284.4 eV. Shirley backgrounds were subtracted from the raw data with the software package Casa XPS vs. 2.3. The X-ray diffraction **(XRD)** of diatomaceous earth and as-purified samples was performed using D8 Focus diffractometer of BRUCKER with copper anticathode (kα1 = 1.5406 A), 40 kV voltage and 40 mA current. The XRD patterns were acquired for 2θ angles ranging from 20˚ to 80˚, with 0.02˚ steps at ambient temperature. The experiments with diffuse reflectance infrared Fourier transform spectroscopy **(DRIFT)** have been performed in a Vertex 70 Bruker IR spectrometer equipped with a one-pot sample compartment. A controlled temperature reaction home-made chamber (7 ml) has been used instead of high-temperature chamber from Harrick, fitted with ZnSe windows and a Praying Mantis diffuse reflection accessory (Harrick). Spectra with Attenuated Total Reflectance **ATR** were conducted by Thermoscientific spectrometer with DTGC KBr detector and KBr separator to identify chemical functional groups present in diatom samples.

3. Diatom Purification Protocols

Concerning fossilized remnants of diatom which is extracted from outer earth's crust, impurities are mainly terrigenous (orthoquartzite, arkose, …), calcareous, metal carbonates and sulfates, sodium chloride, aluminosilicate and metal oxides (Fe, Mg, Ca, …). According to the supplying origin and previous investigations [28], diatomite raw material contains different classes of impurities, as quartz and calcium oxide mainly. For the algal paste, preserved dead cells of diatoms

are enclosed inside bio-silica structure and are considered as impurities. Two different purification protocols to remove impurities from fossilized diatoms and algal paste are required and will be detailed in the following sections.

3.1. Diatomite Raw Rock Purification

Diatomaceous earth contains from 70% to 90% of amorphous silica of *coscinosdiscus lineatus nitudus sp*. XRD of diatomite raw rock is presented latter in **Figure 2** and shows two main impurities: quartz (crystalized silica) and calcite (calcium carbonate). The main problem is inertness of quartz towards chemical attacks and its higher density compared to diatomite amorphous silica. A solution to eliminate it is differential sedimentation in order to split it from diatomite shell. Purification protocol is conducted within two times: first, acid hydrolysis with nitric acid followed by a two-step protocol of differential sedimentation. Briefly, few pieces of diatomite raw rock are ground in a mortar and 5 g of obtained fine powder is homogenously dispersed in 300 mL of HNO_3 solution at 30%wt at room temperature during 17 h. The supernatant is removed and diatomite frustules are subsequently washed with deionized water until pH 7. Later, quartz is eliminated with repeated sedimentation steps as mentioned in **Figure 1**. Samples S1, S2 and S3 are subsequently dried and ground then conserved for further characterization. HNO_3 cleaning protocol is developed regarding two approaches: 1) diatomaceous earth chemical sensitivity toward nitric acid: regarding cited impurities, only non-siliceous materials are dissolved in nitric acid
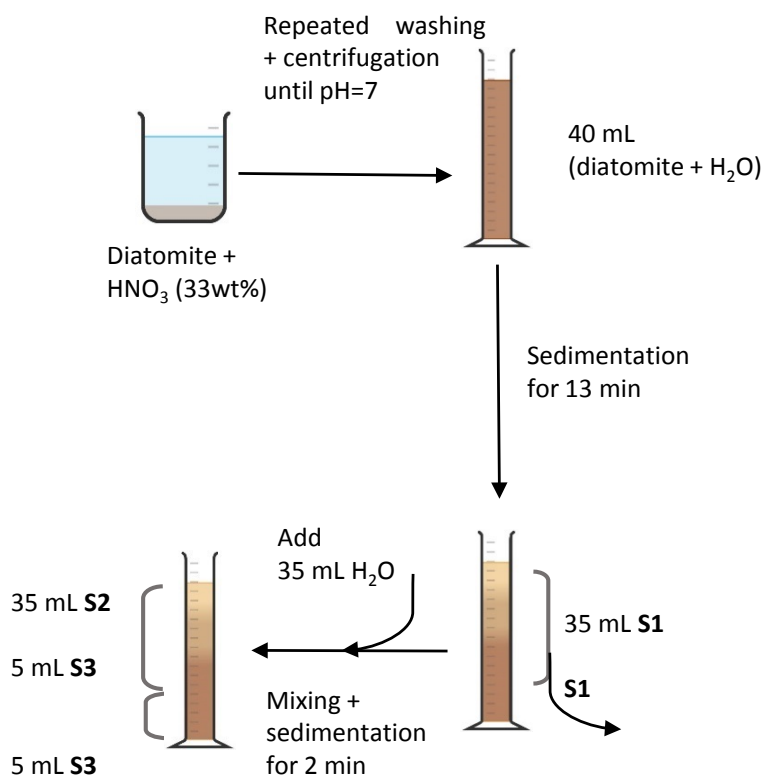

Figure 1. (Chemix) Purification protocol steps of diatomite raw rock.

bath. Secondly, remained materials after acid attack are separated after due to 2) differential sedimentation velocity of amorphous SiO_2 (diatomite frustule)/crystalized SiO_2 (quartz): since quartz density is higher than diatomite frustules, two sedimentation time durations were respected (13 min than 2 min). Collected samples contain decreasing amount of quartz from S1 to S3.

3.2. Diatom Algal Paste Purification

Several studies are currently being carried out on diatom taxa as a source of nutrition for shellfish. In particular, the Institut Français de Recherche pour l'Exploitation de la Mer IFREMER has expertise in diatom aquaculture and bloom with a control of diatom strains [29]. By similarity with our diatomaceous earth material, we studied the purification of *Thalassiosira weissflogii* (TW) sample grown for the larval industry. However, for our purpose which is recovering the silica part only, IFREMER sample concentration on frustule weight is too low (~100 mg/L) to extract enough frustule mass for characterization, surface modification and so on. We therefore selected algal paste since it is much more concentrated than the IFREMER sample (24 g/L toward 100 mg/L), with a narrow distribution in terms of strain and frustule size [30]. In this section, several cleaning protocols for diatom algal paste were undergone and described as well as the infrared ATR characterization corresponding results to check residual organic staff signature.

Algal paste purification steps are reproduced by Table 1 and one step could be described as follow: 5 mL of TW algal paste is dispersed in 15 mL of deionized water and stirred for 5 min at precised temperature. Some amount of HNO_3 (65 wt%), ammoniac (35 wt%) or acetone (90 wt%) according to chosen protocol as mentionned in Table 1, is added dropwise and stirred at 350 rpm during 17 h at corresponding temperature. At the top, mixture colour turns from brown to yellow-green, white or is unchanged according to conducted protocol steps. Diatom frutules are sedimented at bottom and are subsequently washed with deionized water and centrifugated until pH 7, then stored in deionized water for a total volume of 5 mL. Purification step protocol (Table 1) could be followed by a complementary chemical treatment (2 purification steps) or/and thermal treatment (1 purification step). Concerning D12 scale-up experiment, 25 mL of TW algal paste is dispersed in 75 mL of deionized water.
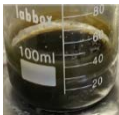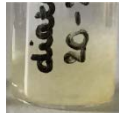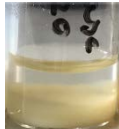
4. Materials Characterization

4.1. Diatomaceous Earth

4.1.1. XRD

XRD patterns obtained by copper anticathode of diatomite raw rock, S1, S2 and S3 are given by Figure 2 to check crystallized impurities presence in raw state and how much cleaning protocol was efficient to eliminate it. Two major phases are detected on raw diatomite rock which are quartz and calcium carbonate according to annotated pic in Figure 2. The peaks at 20.94°, 26.77°, 36.70°, 42.70°,

Table 1. Purification protocol steps for diatom algal paste.

sample ID	purification protocol	Colour of diatom solution	Organic residue after purification (ATR)	Morphology (SEM)
D0 (reference)	heating at 100˚C	brown	Yes	------
D1	1 step 80 mL HNO_3	brown	Yes	------
D2	1 step 80 mL HNO_3 + 1 step 160 mL HNO_3	White-yellow	No	------
D3	1 step 160 mL HNO_3 at 65˚C	green	No	------
D4	1 step 160 mL HNO_3 at 65˚C + calcination at 300˚C for 2 h	White-yellow	No	------
D5	1 step 160 mL HNO_3 at 0˚C	White-yellow	No	smashed
D6	1 step 160 mL HNO_3 at 0˚C ungrounded	White-yellow	No	entire
D7	1 step 160 mL HNO_3 at 0˚C ungrounded + calcination at 300˚C	White-yellow	No	------
D8	1 step 40 mL ammoniac (T_{amb})	Green-brown	Yes	------
D9	1 step 40 mL HNO_3 at 50˚C	Yellow	No	------
D10	1 step 20 mL HNO_3 at 0˚C + 20 mL acetone (T_{amb})	Brown	Yes	------
D11	1 step 20 mL HNO_3 at 0˚C + 20 mL ammoniac at 35˚C	Yellow	No	-------
D12	1 step 20 mL HNO_3 at 0˚C + 20 mL ammoniac at 0˚C	White-Yellow	No	Entire
D12 scale-up	1 step 200 mL HNO_3 at 0˚C + 200 mL ammoniac at 0˚C	White	No	----
D13	IFREMER sample HNO_3	Yellow/white	No	Entire

46.02˚, 50.21˚, 55.08˚, 60.10˚ and 68.34˚ refer to quartz phase while peaks at 23.30˚, 29.52˚, 30.88˚, 36.08˚, 39.62˚, 43.42˚, 47.73˚, 48.62˚, 56.82˚, 57.61˚, 60.70˚, 64.92˚ and 65.71˚ refer to carbonate calcium phase when comparing results with
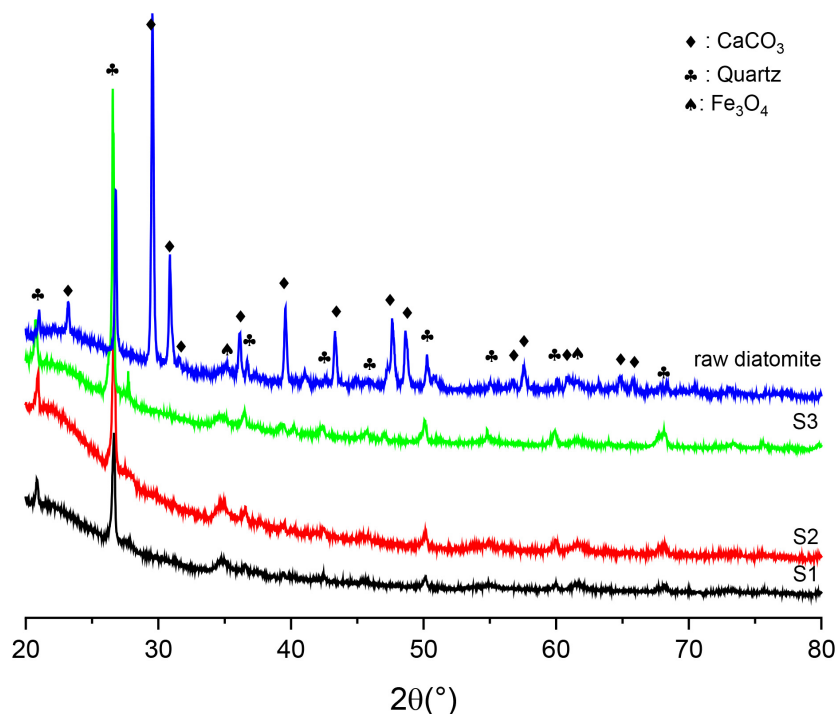
Figure 2. XRD patterns of diatomite raw rock and its purification samples S1, S2 and S3.

standard data of JCPDS n° 03-065-0466 and JCPDS n° 01-085-1108 for the same source. Magnetite phase is probably present in raw rock diatomite since two peaks are detected at 35.26° and 61.83° when comparing to standard data of JCPDS n°01-089-0951 of Fe_3O_4. The absence of calcium carbonate peaks on samples S1, S2 and S3 proves that cleaning protocol was efficient to dissolve $CaCO_3$ by nitric acid attack. The latest is not harvest enough to dissolve quartz, differential sedimentation helps to split major part of it and neglected amount remains in sample S1. For S1, S2 and S3, few peaks of remaining quartz are observed in **Figure 3** patterns for all cited peaks previously with decreasing intensity from S3 to S1. Quartz has a crystalline structure so sharp XRD peaks contrarily to diatom frustules made of amorphous silica corresponding to large shoulder around 20°.

4.1.2. DRIFT

Concerning calcium carbonates, according to **Figure 3**, large band centred at 1430 cm^{-1} on raw rock spectra is assigned to COO asymmetric stretching modes, sharp band at 877 cm^{-1} belongs to out-of-plane bending mode and weak vibration at 717 cm^{-1} belongs to in-plane bending mode [31] [32]. These specific bands of calcium carbonate are observed only on raw diatomite and no traces are observed for purified diatomite sample S1. Thus, HNO_3 protocol is efficient to eliminate calcium carbonate. Silica vibration modes are observed clearly [25] for all sample spectra in **Figure 3**. The intense bands at 1063 and 790 cm^{-1} for raw rock diatomite and S1 to S3 are attributed to bending vibration and symmetric and asymmetric stretching vibration of Si-O-Si network and shoulder at
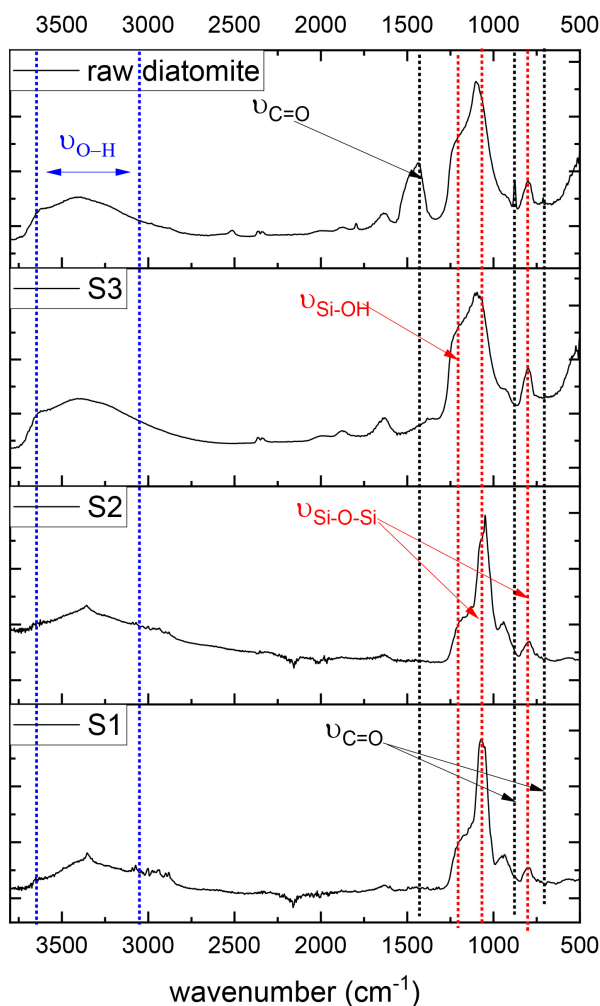
Figure 3. Infrared spectra of diatomite raw rock, S3, S2 and S1.

1150 - 1250 cm^{-1} characterize surface Si-O stretching vibration [17] [33] [34] [35]. Silica networks bands are specific not only for diatom frustules in our context but also to quartz structure. A significant difference could be noted in band intensities ratio of [1150 - 1250 cm^{-1} shoulder intensity/1063 cm^{-1} intensity] ratio (dotted lines in **Figure 3**) between S1 spectra in one hand and raw rock diatomite, S2 and 3 in other hand. This ratio is the lowest for S1 spectra which could be correlated to reduced quartz phase as explained by Meyer-Jacob *et al.* [36]: surface Si-O groups density is higher in case of crystallized phase. Broad band at 3100 - 3690 cm^{-1} for all samples belongs to hydroxyls groups including H-OH for adsorbed water on silica surface in addition to Si-OH groups.

4.1.3. SEM

SEM images of raw diatomite (a, b, c) and purified diatomite S1 (d, e, f, g) of *Coscinosdiscus sp.* [4] are given by **Figure 4**. In icons a, d and e, two overlapping valves with 60 μm of diameter and its girdle bands of 10 μm of width are clearly seen. The successive silica layers separating the hexagonal chambers can be distinguished in caption f. According to icons a, b and c of the same figure,
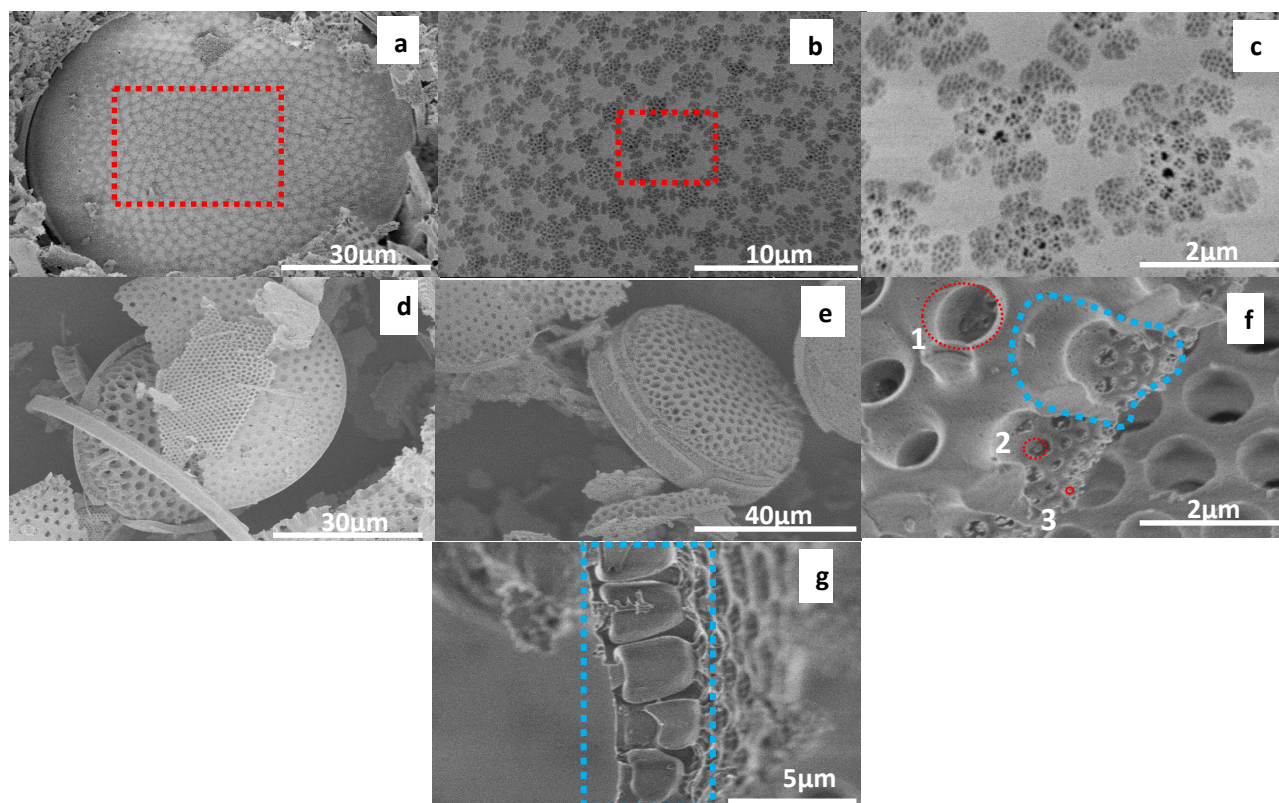
Figure 4. SEM images of diatomite raw rock (a, b, c) and its purified sample S1 after purification protocol (d, e, f, g), (images by Hitachi SU8010).

the cribellum, the outer face has the finest pores with 50 nm of diameter approximately. In contrast, foramen, the inner face, in **Figure 4(f)**, has the largest pores with 1 μm of diameter roughly. Cribrum plate which is the intermediate layer could be distinguished (**Figure 4(f)**) by the intermediate pore size (dotted circle, 2) located between the largest one (dotted circle, 1) of foramen and the finest one (dotted circle, 3) of cribellum. Morphological observation of this diatomite sample and its main strain are coherent with studies of Hadjadj Aoul O. *et al.* [26], and *Vanden Broeck J. et al.* [27]. *Areola chamber is observed in* **Figure 4(f)** *and zoomed in* **Figure 4(g)** (*blue dotted line*) *as a connecting channel between external and internal valve face. Some other references about Coscinodiscus species* [6] *are also in line with this description about inner and outer pore size* [7] [37]. Losic *et al.* [7] made a description of 3 superposed silica layers of diatom frustule (external, intermediate and internal layers) in hierarchical architecture and **Figure 4(f)** confirms it (enclosed pores in dotted red circles) within funnel structure and decreasing pore diameter from inner face to outer face. More details of this material are done on by a combination of tomographic techniques [4]. This observation could be explained by diatom frustules formation timescale: during diatomaceous earth genesis, organic cell is decomposed and separated from silica shell over long timescale during sedimentation in marine basin.

4.1.4. N$_2$-Adsorption

Purified sample S1 undergoes nitrogen adsorption-desorption for calculation of specific surface area (m^2/g) and pores volume according to BET and BJH methods respectively. Isotherm plot is given by **Figure 5** and it can be classified as a IV-type isotherm [38], specific for mesoporous material, on the basis of the International Union of Pure and Applied Chemistry (IUPAC) classification. **Table 2** summarizes specific surface area, S$_{BET}$, and total pores volume, V$_{pores}$, values for raw diatomite and as-purified samples.

Considering isotherm plots of purified diatomite S1 (**Figure 5**) and porosity data (**Table 2**), we can conclude that diatom frustules are considered as multi scale porous material with broad distribution of pore size centred at 50 nm and mesopores appears the major class. Regarding S$_{BET}$ and V$_{pores}$ evolution between raw diatomite and as-purified samples S1, S2 and S3, it's obvious that calcium carbonate dissolution after nitric acid attack helps to remove impurities from total pores and non-porous quartz split after differential sedimentation enhances specific surface area value. A great care must be taken concerning the pore size

Table 2. N$_2$ adsorption-desorption measurements for specific surface area and porous volume calculation for diatomite raw rock and its purification samples (S1, S2 and S3).

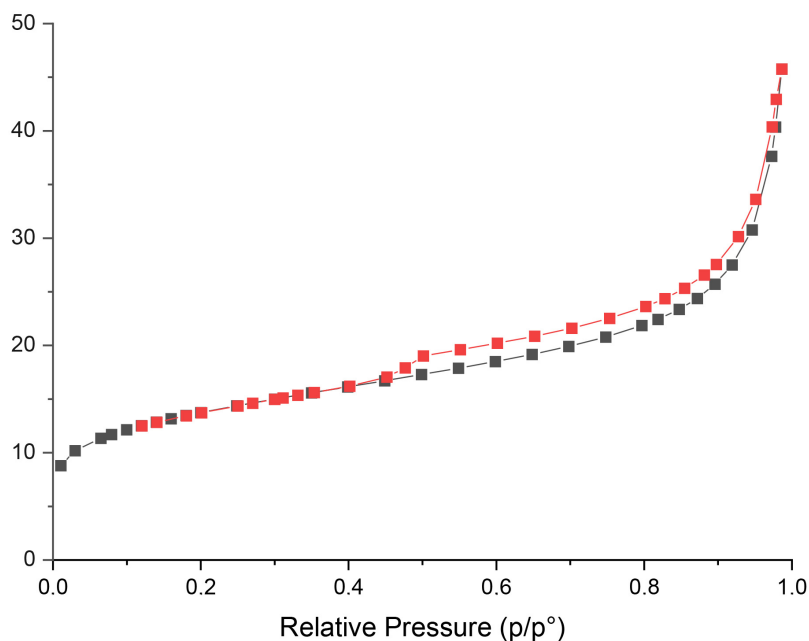| sample	S$_{BET}$ (m^2/g), R^2	V$_{pores}$ (cm^3/g)	Pore diameter (nm)
Diatomite raw rock	27, R^2 = 0.9997	0.043	50
S1	47, R^2 = 0.9995	0.062	50
S2	31, R^2 = 0.9995	0.036	50
S3	25, R^2 = 0.9998	0.058	50

Figure 5. N$_2$-adsorption isotherms of purified diatomite S1 (adsorption in black and desorption in red) with pore size distribution in loop.

distribution around 3.8 nm, which is, as expected by De Lange *et al.* [39] and Groen *et al.* [40], due to the so called tensile strength effect (TSE). TSE is confirmed also by the forced closure of the desorption branch near (p/p°) = 0.42. When considering S_{BET} and V_{tot} values for all samples, diatom frustules have basically low specific surface area and pores volume apparently.

4.1.5. EDX

Topographic observations by SEM are coupled to Energy Dispersive X-ray spectroscopy (EDX) analysis to evaluate chemical composition of raw diatomite and as-purified samples S1, S2 and S3. A current voltage of 15 kV has been applied on frustule surface to measure chemical species over thickness of 3 μm before and after HNO_3 purification protocol. The EDX analysis gives details of the elemental composition (Table 3) of raw diatomite and as-purified frustules. Regarding oxygen (O, ~70%) and silicium (Si, ~28%) distribution, silica structure is confirmed with Si/O ratio is close to 1/2. For carbon (C) and sodium (Na), their presence could infer contamination related to human manipulation and carbon layer deposit for EDX analysis. Other elements with trace composition were; calcium (Ca), magnesium (Mg), potassium (K) and iron (Fe) and chlorine (Cl). For these elements, atomic percentage distribution varies slightly from one sample to another. Lewin J. C. and co-authors [41] consider that some metal cations, especially Al and Fe may be adsorbed onto diatom frustule walls during silica precipitation process by diatoms, radiolarian, sponges, etc. We have noted in our current work that the presence of residual iron oxide layer on frustule, not located on all the part of the frustule but mainly on cribrum/foramen. Iler R.W and al. [42] consider that diatom frustules have similar properties as silica gel regarding specific surface area and their siliceous skeletons act as ion-exchangers. Other references [43] [44] strengthen this thesis and stressed that various metal ions such as Al, Fe, Mg, Ca surface adsorption onto biogenic frustules is possible when taking into account temperature and pH conditions in aqueous media of frustule diatom generation. Hydrochemical and sedimentological environments [45] of the transformation were deeply related to biogenesis of diatom frustules and adsorbed cations.

4.1.6. XPS

Concerning the surface composition of the raw rock diatomite and as-prepared purification samples, XPS data are shown in Figure 6 and the surface chemical

Table 3. Averaged atomic percentage concentrations major elements in dried raw diatomite, S1, S2 and S3 by EDX analysis.

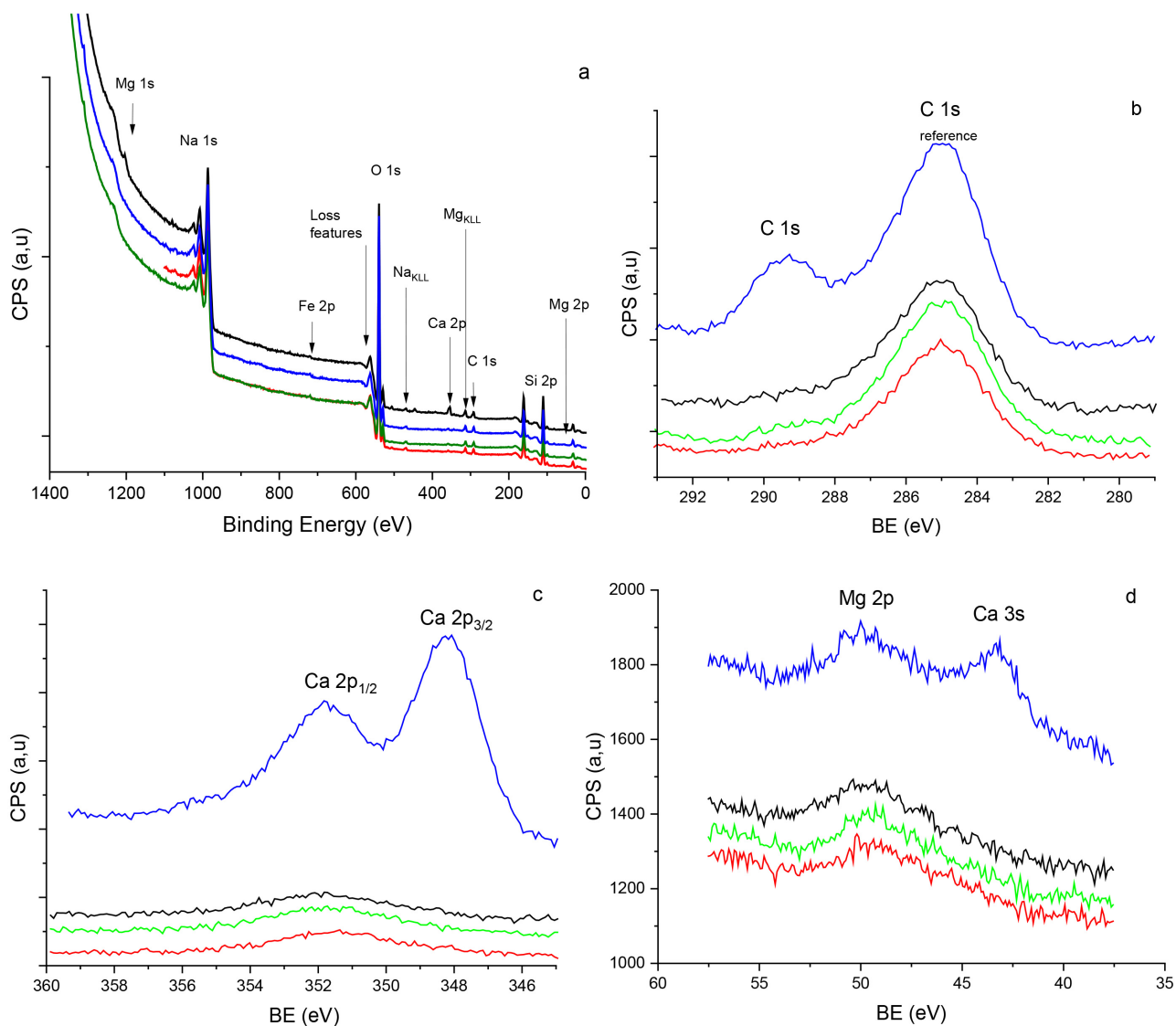|	O	Na	Mg	Si	K	Ca	Fe
raw rock diatomite	71.19	0.19	0.22	27.32	0.02	0.54	0.02
S1	69.11	0.30	0.26	29.21	0.11	-	0.12
S2	72.44	0.26	0.24	26.17	0.07	-	0.09
S3	67.47	0.21	0.19	30.68	0.09	0.28	0.13

Figure 6. Overview XPS spectra (a) C 1s (b), Ca 2p (c) and Mg 2p (d) core level spectra of diatomite raw rock (blue), S1 (black), S2 (red) and S3 (green).

distribution at the surface (maximum ca. 10 nm depth) is summarized by **Table 4**. Overview of the overlapped spectra (**Figure 6(a)**) demonstrates that purification samples and raw rock diatomite have some similarities concerning their chemical composition. Intense pics arising from Si and O core levels are clearly discernible at 103 and 532.5 eV respectively which is coherent with previous analysis (XRD, DRIFT and EDX) and samples type (silica mostly). The full width at half maximum (FWHM) of the O 1s photoelectron line at 532.5 eV has a standard deviation of 0.03 eV in the different samples, which is quite acceptable and confirms that O-Si bond has the major contribution for all samples even for raw diatomite. An intense pick at 1008 eV is attributed to Na 1s core level which usually due external pollution residues. Auger lines Mg_{KLL} and Na_{KLL} are observed at ca. 313 and 500 eV respectively. For carbon C1s photoelectron lines (**Figure 6(b)**), in addition to the adventitious carbon component at 285.5 eV

Table 4. Surface chemical distribution (atomic %) of S1, S2, S3 and raw rock diatomite samples by XPS analysis.

Samples	O 1s % atm	Si 2p % atm	Mg 2p % atm	Ca 2p % atm	C 1s % atm	Fe 2p % atm
raw diatomite	67.80	26.41	1.73	1.82	1.95	0.29
S1	69.36	27.66	1.89	--	0.54	0.28
S2	69.81	27.32	1.84	--	0.46	0.30
S3	69.89	26.96	1.86	--	0.63	0.37

detected for all samples, an additional peak at 298 eV appears for raw rock only. Additionally, the Ca 2p peak has a clear doublet contribution (Ca $2p_{1/2}$ at 348.1 eV and Ca $2p_{3/2}$ at 351.7 eV, Figure 6(c)) only for the raw rock sample. Quantitative calculations for C and Ca prove that their percentages fall from raw rock material to S1, S2 and S3. So, calcium carbonate is eliminated successfully after HNO_3 attack. The Ca 3s peak is displayed in the Mg 2p core level spectra (Figure 6(d)) as a singlet in the low binding energy side for diatomite raw rock only confirming the existence of Ca in this sample. Mg is measured at 2 energy levels: Mg 1s at 1303.9 eV and Mg 2p at 49.4 eV and both of them confirm Mg presence in all diatomite samples. Concerning Mg atomic distribution before and after cleaning, values reported by Table 1 are steady constant around 1.83 atm% ± 0.04. Fe core level at 712.2 ± 0.1 eV for Fe $2p^{3/2}$ [46] has a steady intensity for diatomaceous earth before and after cleaning. XPS quantification for Mg and Fe could be explained by inherent contribution of frustule without impurities.

4.1.7. IGC-Infinite Dilution

The previous results of EDX and XPS investigations on diatomite features before and after purification have demonstrated embedded cations (Mg, Fe, K, Ca) in silica network. These elements are considered as impurities regarding their weight distribution and could tailor diatomite surface properties, as Lewis acidic and basic behaviour namely. To go further and deepen this concept, IGC has been conducted on raw rock diatomite and S1 samples to characterize Lewis acidity and basicity which are compared to ultra-pure silica gel (SiO_2 100%) purchased from Sigma (Merck). Supercritical process was used for solvent removal from silica gel structure (according to supplier specifications product form) and the highest temperature applied should range between 30°C and 80°C [47] [48]. Both bio-silica samples and silica gel sample undergo the same highest heat treatment temperature during IGC analysis at 200°C and they are characterized without additional surface treatment. IGC-infinite dilution is convenient to highlight diatomite peculiarity because it is based on diatomite surface-molecular probe interaction study to determine only Lewis properties contrarily to chemisorption analysis that is dedicated to Lewis and Brønsted properties. Lewis acidity and basicity concepts used by ICG are based on Gutmann [49] [50] and Van Oss [51] approach as detailed in the following equation:

$$\Delta G_{ads}^{SP} = K_A \cdot DN + K_D \cdot AN$$

where ΔG_{ads}^{SP} is the free enthalpy of sorption of a polar probe molecule, K_A is the electron-accepting (acid) number of the solid surface, K_D is the corresponding electron-donating (base) number. DN and AN are defined by Gutmann as quantitative measure of donor number (Lewis basicity) and acceptor number respectively of polar probe. Gutmann's numbers were employed accurately to quantify several polar probes [52] [53]; for example DN/AN ratio is 4.9 for diethyl ether because of oxygen lone pair (Lewis basicity) but for benzene DN/AN ratio value is roughly 0 because of electronic acceptor character of aromatic ring. K_A and K_D values can be extracted from the slope (and the intercept of linear plot ΔG_{ads}^{SP} /AN vs. DN/AN [54]. **Figure 7** illustrates this correlation for raw rock diatomite, S1 and ultra-pure silica gel. For K_A and K_D values (**Table 5**), the K_A/K_D is considered to deduce an acidic property of material surface when its value is higher than 1 and should indicate a basicity character of material surface when its value is lower than 1.

When observing K_A/K_D ratio, silica gel surface is considered as acid with $K_A/K_D = 2.1$ while diatomite raw rock and S1 materials are almost basic with 0.9

Table 5. K_A and K_D constants issued from the linear plot of ΔG_{ads}^{SP} /AN vs. DN/AN.

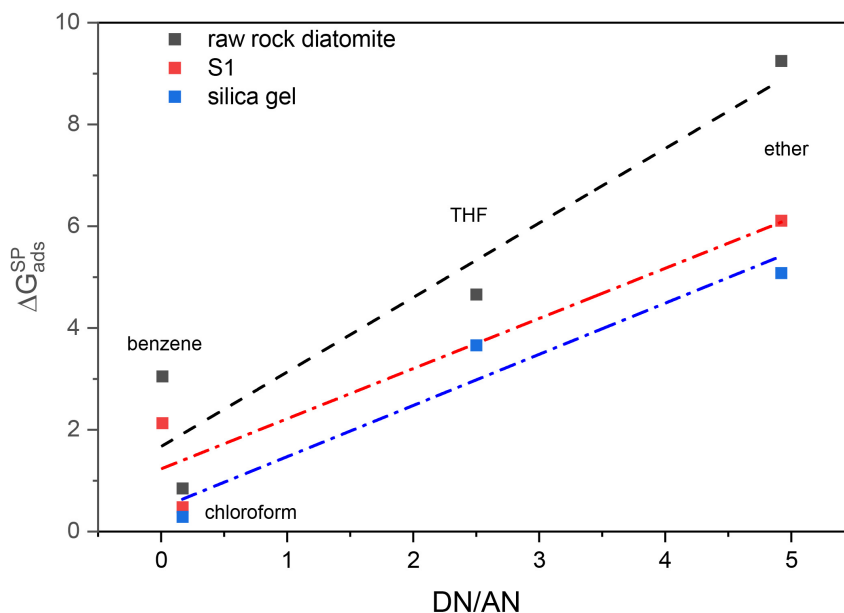| sample	K_A	K_D	K_A/K_D
Raw diatomite ($r^2 = 0.85$)	147.5	161.6	0.9
S1 ($r^2 = 0.90$)	98.5	123.0	0.8
Silica gel ($r^2 = 0.94$)	100.4	47.2	2.1

Figure 7. Determination of Lewis acidity (K_A) and basicity (K_D) constants with IGC for raw rock diatomite (black square), S1 (red square) and silica gel (blue square) using linear plot ΔG_{ads}^{SP} /AN vs. DN/AN, ($\Delta(\Delta G_{ads}^{SP}) < 2\%$).

and 0.8 respectively. K_D constants for diatomite features are, at least, 2 times higher than silica gel one. So, diatomite frustules are clearly more basic than pure silica.

4.2. Diatom Algal Paste

4.2.1. Infrared ATR

Infrared spectra of original algal paste and selected purified samples presented by Table 1 are shown by Figure 8. Some similarities are highlighted concerning silica network assignment bands [25]. As detailed for diatomite raw rock DRIFT spectra, intense band at 1063, 798 and 447 cm^{-1} are attributed to bending vibration and symmetric and asymmetric stretching vibration of Si-O-Si inner network bonds [17] [34] while shouldered band at 1150 - 1250 cm^{-1} refers to Si-O out-of-phase stretching vibration [33]. Band at 948 cm^{-1} detected in all spectra except for raw algal paste (D0) described Si-O stretching vibration of silanol groups [55]. All silica network bond assignments are detected with more or less magnitude according cleaning process. For D0 spectrum, silica bands are relatively lower or/and masked with organic matter bands. For D6, D7, D9, D10,
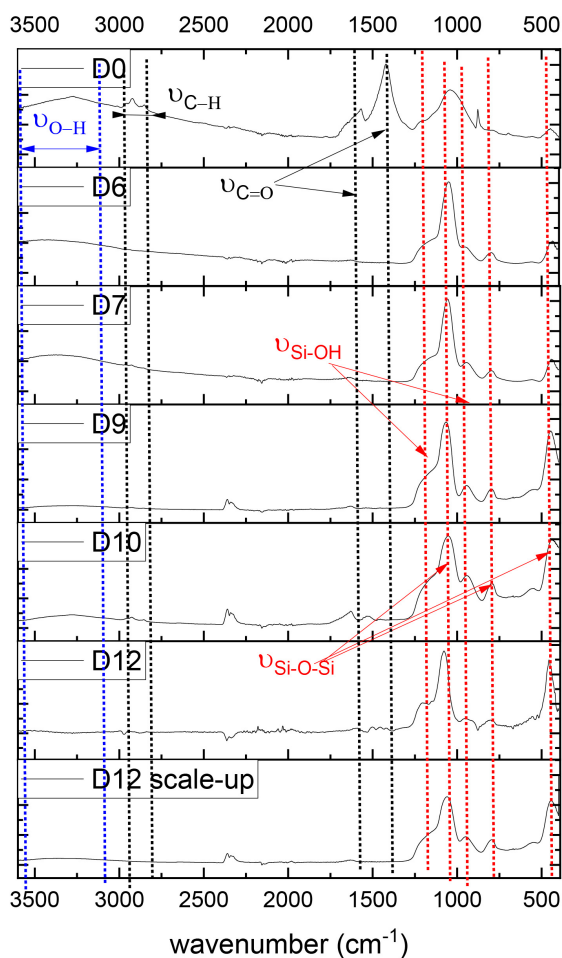

Figure 8. ATR spectra for diatom algal paste and selected purified samples as described by Table 1.

D12 and D12 scale-up spectra, it could be assumed that bending and stretching vibration at 1063 cm^{-1}, 798 and 447 cm^{-1} have approximately the same shape and intensity. Nevertheless, silanol groups contribution intensity at 948 cm^{-1} is higher with two steps cleaning process for D9, D10, D12 and D12 scale-up samples. This observation could be explained by sample dehydration state (drying temperature before and/or during ATR measurement since some samples are exposed to ambient atmosphere during short or long timescale before ATR measurement). For D6 and D7 samples, large band centred at 3340 cm^{-1} is more intense for D6 and D7 samples, and is contribution of hydroxyls moieties –OH of H_2O and Si-OH bonds. Organic matter which is the impurity to split for diatom algal paste has some representative bands vibration at 2940 - 2840 cm^{-1} for C-H stretching vibration, 1565 and 1427 cm^{-1} for C=O stretching vibration mode. These vibrations are clearly observed for raw diatom algal paste sample D0 and fewer of them with lower intensity for D9 and D10 samples. Absence of organic matter bands could be confirmed for D6, D7, D12 and D12 scale-up samples. Process cleaning for D6 and D7 used high HNO_3 amount while D12 one is made in two steps with eight time lower HNO_3 amount followed by NH_3 bath. It is well known that cell exposed to alkali agents as ammonia lead to protein denaturation and lipid saponification [56], that's why using NH_3 enhances organic matter dissolution without requiring important chemical reagents volume.

4.2.2. SEM

SEM images are done for purified IFREMER and algal paste samples once ATR analysis validates the absence of organic matter. Microscopy investigation for algal paste samples is a relevant step in order to evaluate which purification protocol is efficient enough to keep intact diatom frustules in box aspect (overlapping valves with surrounding girdle intact). SEM images for *Thalassiosira weissflogii* strain are given by Figure 9 for IFREMER (a) and algal paste samples (b to h). It can be easily confirmed that majority of frustule box of *Thalassossira weissflogii* strain are non-smashed (Figures 9(a)-(c)) and their 3D nanostructure are entirely conserved after undergoing purification protocol. Valves and girdles bands are maintained together (Figure 9(e)) and for some opened diatom box, inner face is presented by icon Figure 9(g) and outer face by Figure 9(d). The pores, for both of them, appeared free of biomass in icons Figure 9(f) and Figure 9(h). According to the last two figures, the outer face (cribrum) is with sizing pores diameter 60 nm approximately (Figure 9(f)) while the inner face (cribellum) has the finest pores measuring 40 nm roughly (Figure 9(h)). This organization for pores size between sieve frustule plates is confirmed by previous work [7] and is quite opposite for that of Coscinodiscus sp. observed in diatomaceous earth. What is noteworthy in algal paste studies compared to the existing literature is the obtaining of a homogeneous batch of frustules issued from the same taxon with limited damaged pieces.
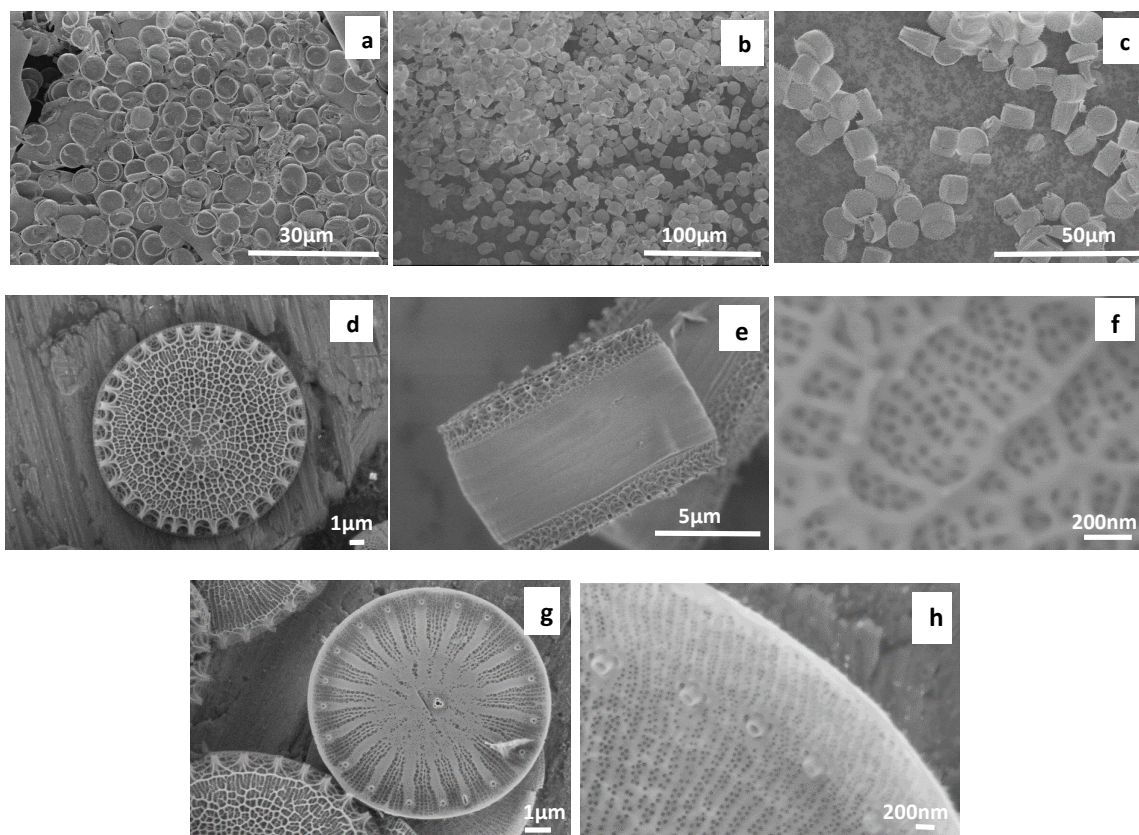
Figure 9. SEM images of *Thalassiosira weissflogii* sp. of IFREMER sample D13 (a) and algal paste samples D6 (b, c, e) and D12 (d, f, g, h), (a, b, c, e by Hitachi SU8010; d, f, g, h by Zeiss 2600F).

4.2.3. XPS

Carbon and nitrogen are the most representative elements of biomass. XPS measurements of frustule surface for contaminated diatom (D5 and D10) and pure diatom (D12) after undergoing corresponding cleaning process is conducted to confirm previous results. Overview of overlapped spectra (**Figure 10(a)**) demonstrates that diatom samples have similar chemical composition globally. Intense pics arising from O and Si core levels are clearly discernible at 103 and 532.7 eV in **Figure 10(a)** which is coherent with previous analysis and samples type (silica mostly). FWHM of O 1s electron line (**Figure 10(b)**) at 532.7 eV has a standard deviation of 0.04 eV so main O is bonded to Si in silica network. Regarding carbon and nitrogen contents (**Table 6**), it can be concluded that two step cleaning protocol using HNO_3 followed by NH_3 attack is efficient to dissolve all organic matter of living diatom. C 1s peaks (**Figure 10(c)**) of D5, D10 and D12 have asymmetric shape, which can be attributed to C-O, C=O and O-C=O [57] bonds contribution in the high binding energy side.

5. Discussion

HNO_3 purification protocol coupled to sedimentation for diatomaceous raw rock was efficient to eliminate calcite but some quartz is remained in the cleanest sample, S1. This result was confirmed by XRD pattern (**Figure 2**) in addition to
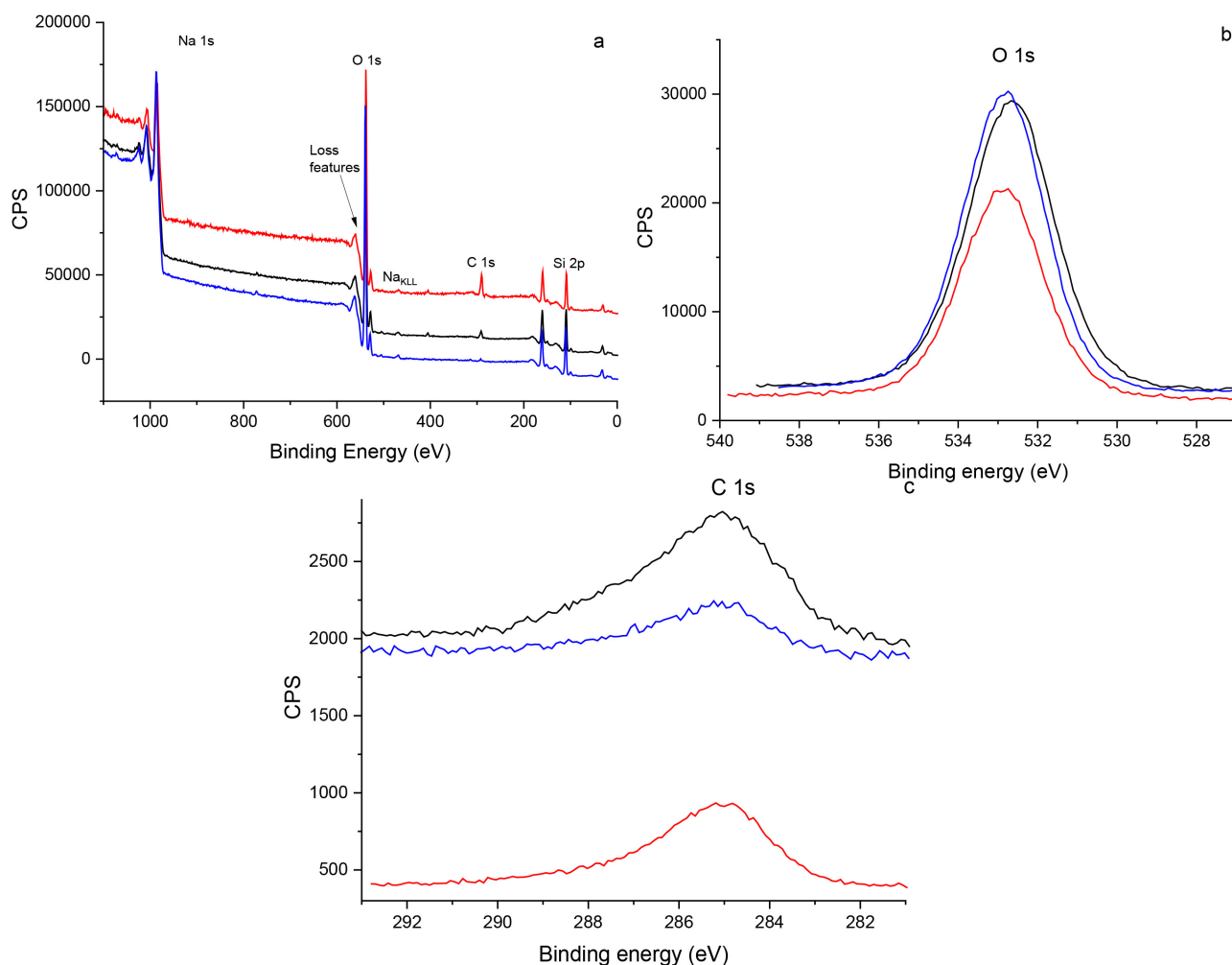
Figure 10. Overview XPS spectra (a) O 1s (b), Si 2p and C 1s (c) and core level spectra of treated algal paste samples D5 (red), D10 (black) and D12 (blue).

Table 6. XPS element measuring of D5, D10 and D12 diatom algal paste purification samples.

	O % atm	Si % atm	C % atm	N % atm
D10	60.59	31.44	6.71	1.26
D5	56.53	24.70	17.44	1.34
D12	65.44	31.88	2.69	0.00

DRIFT spectra (**Figure 3**) since calcite signature disappeared totally in S1, S2 and S3 samples. Elemental composition of diatomite raw rock and as-purified samples has been evaluated by EDX and XPS. Before and after purification steps, Mg presence has been confirmed by EDX and XPS analysis mutually at different atomic averages and supports the adsorption of Mg cations in frustule walls during silica biogenesis. The same conclusion could be done for Fe since its atomic concentration is steady before and after cleaning protocol according to quantitative results of EDX (**Table 3**) and XPS (**Table 4**). Concerning Ca, only

quantitative analysis by EDX for S3 confirms its presence at 0.28 atm%. Potassium (K) has been detected by EDX for purified samples S1, S2 and S3 only and no traces by XPS investigations. These differences about Mg, Ca, Fe and K sensitivity and concentrations accuracy between EDX and XPS results are due to analytical specifications for these two characterization methods for instance. EDX scanning dimension spot are 30 μm × 36 μm on frustule surface and 3 μm of thickness while XPS scanning spot dimensions are too smaller (5 nm × 5 nm) and for 10 nm of thickness only. In addition, XPS analysis are averaged over a sample mass (few mg) while EDX quantification results are reported for one frustule. Nevertheless, these two investigations confirm cations adsorption in bio-silica frustule network during its biogenesis which is largely demonstrated [43] [44]. Thus, remaining amounts of Mg, Ca, K, Fe and Ca in samples after HNO_3 cleaning protocol and differential sedimentation emphasize these cations are intrinsically adsorbed in 3D intricate architecture of diatom frustules and considered as doping element. To deepen this doping effect and highlight diatom feature peculiarity toward synthetic silica, IGC-infinite dilution investigations has been done for raw rock diatomite, as-purified sample S1 and ultra-pure synthesized silica to evaluate its acidic K_A and basic K_D Lewis properties. A basic behaviour was proven for diatomite materials in comparison to synthetic silica which is due to embedded cations as Mg, Ca, and Fe mainly. This is coherent with mass composition of S1 bio-silica (SiO_2 98 wt% in bulk according to EDX results and SiO_2 96 wt% at 10 nm depth according to XPS results) in comparison to silica gel (SiO_2 100 wt%). Embedded Mg, Ca and Fe cations in bio-silica network are involved in electronic structure: these cations replace Si cations and regarding their electronegativity difference toward Si, electronic cloud of cation-oxygen covalent bond is then more focused around oxygen lone pair. So, oxygen basicity is enhanced and diatom frustules could be convenient if silica material is seeked with moderate acidity.

For porosity investigations, SEM captions in Figure 4 presented clearly the hierarchical porosity of frustule in diatomaceous earth in stackable sieve layers in which the finest pores with 50 nm of diameter are in the outside layer and the largest pores of 1μm are in the inner layer. Pores size and its geometrical position in 3 layers to form areola chamber give periodicity to diatomite frustule as described by Mcheick A. *et al.* [58]. N_2-adsorption/desorption for specific surface area determination confirmed SEM investigations: pores distribution according to BJH model for coscinosdiscus sp. is large and centred around 50 nm. Larger pores could not be quantified by N_2 adsorption/desorption technique due to porosity scale. A low specific surface area of 47 m^2/g for purified diatomite, S1, has been calculated which is related to specific hierarchical structure of frustule pattern: mesopores and macropores are the largest type of pores. This frustule property could be considered as an advantage for catalysts used in liquid phase with high molecular weight reactants to avoid limited mass transfer [59]. Moreover, specific surface area could be enhanced artificially by nanoparticles

deposition to meet requested specifications.

Regarding periodicity in morphological structure of diatomite frustule in addition to high index contrast between silica (n ≈ 1.45) and air (n = 1), coscinosdiscus sp are considered as 3D photonic crystal [37]. So frustule features could be used as microlens in light-trapping technologies for high-efficiency thin-film solar cells. A recent study in 2015 by Chen *et al.* [60] about diatomite light-trapping effect proved a remarkable broadband enhancement of absorption in visible spectrum regions and this behaviour was correlated to multiple scattering induced by stackable frustule structure and pore size distribution for each layer. This study highlighted the solution that could be offered by diatomite features to obtain large-scale, ecological and economic light-trapping device. Periodicity of diatomite frustule obtained from mono-strain source of diatom at large scale goes beyond the human know and know-how ability to synthesize regular micro-scale plates for light-trapping technologies since multiple self-assembly methods failed to meet regularity and uniformity requirements [61] [62]. Through XPS and EDX investigations (Table 3 and Table 4), we demonstrated that frustule features are composed of silica network with embedded cations, Mg, Ca, and Fe mainly. Such Mg doped silica materials are recently studied by Nandi M. *et al.* [63] for their catalytic activities in Knoevenagel reaction, a key step for various pharmaceuticals preparation. The prepared materials exhibit high catalytic activity attributed to high mass transfer due to porous structure. To underline possible use of diatomaceous earth frustule intrinsically doped with alkali metals, Mg doped silicon is potential way of frustule upgrade in terms of eventual application in photonic devices operating in the middle infrared spectral range [64]. Other purpose, doped and highly porous structure of diatomite frustule could be a good candidate for efficient and affordable thermoelectric materials for high-temperature use as mentioned by Yabu H. *et al.* [65] in his study about new magnesium silicide films. The latest are obtained by honey comb polymer reduced under Mg vapour to obtain Mg_2Si film over carbon porous structure. Particular thermal properties of obtained material were correlated to porous honey comb structure. Our studied frustule issued from diatomaceous earth could be convenient to replace the used honey comb polymer to obtain Mg_2Si material after magnesio reduction with more ecological and economic way using Bio-clastic and Shape preserving Inorganic Conversion (BaSIC) [66] process. BaSIC is changing the composition of a given pattern while saving their 3D morphologies. This process is being more and more attractive to provide nanostructured devices with complex 3D porous patterns and tuned composition and it was applied to diatom frustules to obtain frustule replicas made of Si, Au or Pd, C or C/Pt, MnO_2, carbon or polymers based replicas [66].

Morphological investigations with SEM has confirmed that purified diatomite sample S1 contains fragmented frustule with different size and shape which may be quite different of scientists' intention to get benefit of entire hierarchical patterns of diatomite frustule to make micro-reactor material. Sieve properties dem-

onstrated by SEM captions in **Figure 4** could be only considered in limited area of fragmented frustules. For that reason, another source of diatomite material was studied in this paper which is diatom algal paste in order to get hole benefit of frustule porosity. Using a micro-structure in as-petri-dish like diatomite overlapping frustules with controlled porosity is a main target of many researchers as in biotechnology applications for therapeutics release in drug delivery and cancer therapy [14].

For algal paste, the purification challenge using two steps protocol (nitric acid-ammonia) at low temperature is consisting on organic cell elimination without damaging the surrounding frustule. This diatom material is issued from *Thalassiosira weissflogii* aquaculture in synthetic seawater. The strain is originated from saltwater lagoon in Hawaii and one of its older name is *Thalassiosira fluviatile*. The quantity of vegetable matter is important (78% of the weight [67] of a diatom) and the treatment must be done carefully in order to save the petri-dish diatom frustule structure. Two main damage risks are considered 1) frustule texture lost by scrubbing effect or fragmentation for example and 2) the overlapped valves opening and girdle dissociation. SEM images for diatom algal paste confirms no scrubbing effect and typical porosity features are preserved after purification protocol. Concerning the second damage, captions b, c and e of the same figure (**Figure 9**) demonstrated that overlapped valves dissociation is not frequent and the decomposition of the organic pattern, lodged in the box, was successfully achieved. In this case, many frustules are observed preserved, even intact.

Elemental composition of frustule pattern is different according to its source: XPS investigations has demonstrated silica network with embedded alkali cations for diatomaceous earth while frustule pattern is composed of pure silica when its origin is algal paste. Diatomaceous earth contains centric *coscinosdiscus lineatus nitudus* as the major strain issued from Marine sediments of Late Miocene while algal paste is resulting of recent (2019) aquaculture of *Thalassiosira weissflogii* in artificial sea water made of fresh water. So both resources are similar concerning salinity level. The main difference is related to cell density which is about 0.32 billion/mL for algal paste while it ranges between 10^6 and 10^7 cells/m^3 for diatom in natural media [68]. So difference in chemical composition between frustules issued from diatomite raw rock and algal paste could be related to metal ions (like Mg, Ca and Fe) availability/cell between diluted (diatomite raw rock) vs concentrated (algal paste) culture media for their adsorption during diatom biogenesis. Diatom frustule issued from algal paste could be a potential candidate for versatile uses when pure silica is requested while doped frustules are convenient for applications mentioned above. In the case of the use of diatomite raw rock, the main majority of frustules are fragmented. It is difficult with this raw material to obtain samples of identical fragments size. On the other hand, with diatoms, it appears possible to have batches of un-damaged frustules of the same size as showed by **Figure 8**: D12 scale-up experiment was

successfully achieved without organic residue to obtain substantial amount of entire frustules with preserved texture and morphology. With algal paste, the distribution of frustules seems very similar in size because of mono-strain source, identically to Ifremer sample (**Figure 9(a)**), however Ifremer sample concentration is not high enough to produce silica material for further applications. For that reason, living algal paste seems to be a convenient and promising source to obtain entire diatom frustules and take advantage of its nano-architecture without losing its native morphology as petri-dish structure.

Optimized purification protocols for diatomaceous earth and diatom algal paste involve nitric acid use at 35 wt% and ammonia at 17.5 wt% in addition to deionized water for neutralization. These concentrations could be reduced or recycled for environmental reasons mainly. Meanwhile, the purification steps detailed in this work could be considered as one of the eco-friendliest process regarding other studies in terms of reagents concentration, intermediate steps number, total purification process timescale, power demand, … [69] [70] [71]. Moreover, the presented purification protocol for diatom algal paste allow access to substantial quantities of mono-strain diatom samples with identical size, shape and micro-porosity, which is highly demanded in all nanotechnology field for versatile applications.

6. Conclusion

Study of bio-silica issued from diatom frustules was deeply conducted concerning morphology, chemical composition, size and shape homogeneity whatever diatom origin was fossil or not. Special considerations were paid to purification protocol efficiency to obtain pure diatom frustules without residual impurities either inorganic or organic. Pure frustules of diatomaceous earth seem to be naturally doped silica with embedded Mg, Ca and Fe mainly according to XPS and EDX investigations which is quite profitable for specific use to obtain doped microporous materials with ecological and economical way. Diatomite raw rock is an abundant source of porous silica but major frustules are fragmented. The second source of bio-silica which is diatom algal paste of unique strain allow access to undamaged frustules with two-overlapped valves and its surrounding girdle with preserved micro-texture after undergoing purification protocol. Scaling up of diatom algal paste purification process was achieved successfully regarding SEM and ATR results which is a potential opportunity to obtain substantial quantity of identical and micro-structured items avoiding the use of costly nanotechnology technics and resource waste.

Acknowledgements

the future". Professor Ouassini HADJADJ-AOUL from University of Algeria is acknowledged for providing diatomaceous earth sample. We are thankful for Pr. Philippe MINER from IFREMER institute for valuable discussions and advices for diatom strain and source choice. Then finally, we thank master students Delphine Larue, Abir Ben Bouzayene and Clara Lauffenburger for their precious contribution.

Conflicts of Interest

The authors declare no conflicts of interest regarding the publication of this paper.

References

[1] Tréguer, P., Nelson, D.M., Van Bennekom, A.J., *et al.* (1995) The Silica Balance in the World Ocean: A Reestimate. *Science*, **268**, 375-379. https://doi.org/10.1126/science.268.5209.375

[2] Granum, E., Raven, J.A. and Leegood, R.C. (2005) How Do Marine Diatoms Fix 10 Billion Tonnes of Inorganic Carbon per Year? *Canadian Journal of Botany*, **83**, 898-908. https://doi.org/10.1139/b05-077

[3] Mansilla, C., Novais, M.H., Faber, E., *et al.* (2016) On the 3D Reconstruction of Diatom Frustules: A Novel Method, Applications, and Limitations. *Journal of Applied Phycology*, **28**, 1097-1110. https://doi.org/10.1007/s10811-015-0653-y

[4] Darouich, O., Baaziz, W., Ihiawakrim, D., *et al.* (2022) 3D Multiscale Analysis of the Hierarchical Porosity in *Coscinodiscus* sp. Diatoms Using a Combination of Tomographic Techniques. *Nanoscale Advances*, **4**, 1587-1598. https://doi.org/10.1039/D1NA00691F

[5] Wang, Y., Pan, J., Cai, J., *et al.* (2011) Assembling and Patterning of Diatom Frustules onto PDMS Substrates Using Photoassisted Chemical Bonding. *Chemistry Letters*, **40**, 1354-1356. https://doi.org/10.1246/cl.2011.1354

[6] Losic, D., Mitchell, J.G. and Voelcker, N.H. (2009) Diatomaceous Lessons in Nanotechnology and Advanced Materials. *Advanced Materials*, **21**, 2947-2958. https://doi.org/10.1002/adma.200803778

[7] Losic, D., Rosengarten, G., Mitchell, J.G., *et al.* (2006) Pore Architecture of Diatom Frustules: Potential Nanostructured Membranes for Molecular and Particle Separations. *Journal of Nanoscience and Nanotechnology*, **6**, 982-989. https://doi.org/10.1166/jnn.2006.174

[8] Zhang, D., Wang, Y., Cai, J., *et al.* (2012) Bio-Manufacturing Technology Based on Diatom Micro- and Nanostructure. *Chinese Science Bulletin*, **57**, 3836-3849. https://doi.org/10.1007/s11434-012-5410-x

[9] Round, F.E., Crawford, R.M. and Mann, D.G. (1990) The Diatoms: Biology and Morphology of the Genera. *Journal of the Marine Biological Association of the United Kingdom*, **70**, 924. https://doi.org/10.1017/S0025315400059245

[10] Sumper, M. (2002) A Phase Separation Model for the Nanopatterning of Diatom Biosilica. *Science*, **295**, 2430-2433. https://doi.org/10.1126/science.1070026

[11] Levitan, O., Dinamarca, J., Hochman, G. and Falkowski, P.G. (2014) Diatoms: A Fossil Fuel of the Future. *Trends in Biotechnology*, **32**, 117-124. https://doi.org/10.1016/j.tibtech.2014.01.004

[12] Shan, R., Zhao, C., Yuan, H., *et al.* (2017) Transesterification of Vegetable Oil Using

Stable Natural Diatomite-Supported Catalyst. *Energy Conversion and Management*, **138**, 547-555. https://doi.org/10.1016/j.enconman.2017.02.028

[13] Lopez, P.J., Desclés, J., Allen, A.E. and Bowler, C. (2005) Prospects in Diatom Research. *Current Opinion in Biotechnology*, **16**, 180-186. https://doi.org/10.1016/j.copbio.2005.02.002

[14] Maher, S., Kumeria, T., Aw, M.S. and Losic, D. (2018) Diatom Silica for Biomedical Applications: Recent Progress and Advances. *Advanced Healthcare Materials*, **7**, Article ID: 1800552. https://doi.org/10.1002/adhm.201800552

[15] Rea, I. and De Stefano, L. (2019) Recent Advances on Diatom-Based Biosensors. *Sensors*, **19**, Article 5208. https://doi.org/10.3390/s19235208

[16] Shi, M., Li, J., Cai, J., *et al.* (2017) Nano Sulfur-Coated Diatomite for Enhanced Chromate Removal by Sulfide Reduction. *Journal of Nanoscience and Nanotechnology*, **17**, 6686-6691. https://doi.org/10.1166/jnn.2017.14474

[17] Jiang, W., Luo, S., Liu, P., *et al.* (2014) Purification of Biosilica from Living Diatoms by a Two-Step Acid Cleaning and Baking Method. *Journal of Applied Phycology*, **26**, 1511-1518. https://doi.org/10.1007/s10811-013-0192-3

[18] Morales, L.V., Sigman, D.M., Horn, M.G. and Robinson, R.S. (2013) Cleaning Methods for the Isotopic Determination of Diatombound Nitrogen in Non-Fossil Diatom Frustules: Cleaning Diatoms for N Isotope Analysis. *Limnology and Oceanography*: *Methods*, **11**, 101-112. https://doi.org/10.4319/lom.2013.11.101

[19] Wang, Y., Cai, J., Jiang, Y., Jiang, X.G. and Zhang, D.Y. (2013) Preparation of Biosilica Structures from Frustules of Diatoms and Their Applications: Current State and Perspectives. *Applied Microbiology and Biotechnology*, **97**, 453-460. https://doi.org/10.1007/s00253-012-4568-0

[20] Delasoie, J. and Zobi, F. (2019) Natural Diatom Biosilica as Microshuttles in Drug Delivery Systems. *Pharmaceutics*, **11**, Article 537. https://doi.org/10.3390/pharmaceutics11100537

[21] Zhang, D., Wang, Y., Pan, J. and Cai, J. (2010) Separation of Diatom Valves and Girdle Bands from Coscinodiscus Diatomite by Settling Method. *Journal of Materials Science*, **45**, 5736-5741. https://doi.org/10.1007/s10853-010-4642-x

[22] Morse, D.E. (1999) Silicon Biotechnology: Harnessing Biological Silica Production to Construct New Materials. *Trends in Biotechnology*, **17**, 230-232. https://doi.org/10.1016/S0167-7799(99)01309-8

[23] Rea, I., Terracciano, M. and De Stefano, L. (2017) Synthetic vs Natural: Diatoms Bioderived Porous Materials for the Next Generation of Healthcare Nanodevices. *Advanced Healthcare Materials*, **6**, Article ID: 1601125. https://doi.org/10.1002/adhm.201601125

[24] Buchner, G.A., Stepputat, K.J., Zimmermann, A.W. and Schomäcker, R. (2019) Specifying Technology Readiness Levels for the Chemical Industry. *Industrial & Engineering Chemistry Research*, **58**, 6957-6969. https://doi.org/10.1021/acs.iecr.8b05693

[25] Gélabert, A., Pokrovsky, O.S., Schott, J., *et al.* (2004) Study of Diatoms/Aqueous Solution Interface. I. Acid-Base Equilibria and Spectroscopic Observation of Freshwater and Marine Species. *Geochimica et Cosmochimica Acta*, **68**, 4039-4058. https://doi.org/10.1016/j.gca.2004.01.011

[26] Hadjadj Aoul, O. (2000) Etude de supports de colonnes chromatographiques à base de matériaux locaux algériens, Algérie. Ecole Nationale Polytechnique. http://catalogue2.biblio.enp.edu.dz/index.php?lvl=author_see&id=7149

[27] Vanden Broeck, J. and Querio, A. (1960) La diatomite (Kieselgur): Les diatomées et

leurs emplois dans l'industrie. 3e Édition.
https://ulysse.univ-lorraine.fr/discovery/fulldisplay?vid=33UDL_INST:UDL&docid=alma991002218459705596&lang=fr&context=L&adaptor=Local%20Search%20Engine

[28] Garnier, A. (2013) Platine sur silice: Exemples réussis de synthèse par voie organométallique pour la catalyse hétérogène: Validation par l'adsorption et la réactivité du CO. Université de Strasbourg.
https://hal.archives-ouvertes.fr/tel-01124197/

[29] Pernet, F., Malet, N., Pastoureaud, A., *et al.* (2012) Marine Diatoms Sustain Growth of Bivalves in a Mediterranean Lagoon. *Journal of Sea Research*, **68**, 20-32.
https://doi.org/10.1016/j.seares.2011.11.004

[30] Kang, J.S., Kim, H.S. and Lee, J.H. (1996) Morphological Variations of the Marine Diatom *Thalassiosira weissflogii* under Culture Conditions. *Algae*, **11**, 23-34.

[31] Lee, S.H., Bae, Z.U., Kim, K.W., *et al.* (1997) Determination of Calcium Carbonate in Limestone by Attenuated Total Reflectance Fourier Transform Infrared Spectrometry. *Analytical Sciences*, **13**, 93-96.
https://doi.org/10.2116/analsci.13.Supplement_93

[32] Youssef, I., Sall, S., Dintzer, T., *et al.* (2019) Forward Looking Analysis Approach to Assess Copper Acetate Thermal Decomposition Reaction Mechanism. *American Journal of Analytical Chemistry*, **10**, 153-170.
https://doi.org/10.4236/ajac.2019.105014

[33] Lettieri, S., Setaro, A., De Stefano, L., *et al.* (2008) The Gas-Detection Properties of Light-Emitting Diatoms: The Gas-Detection Properties of Light-Emitting Diatoms. *Advanced Functional Materials*, **18**, 1257-1264.
https://doi.org/10.1002/adfm.200701124

[34] Li, Y., Chian, W., Wang, X., *et al.* (2011) Coordination Assembly and Characterization of Red-Emitting Europium (III) Organic/Inorganic Polymeric Hybrids: Photochemistry and Photobiology. *Photochemistry and Photobiology*, **87**, 618-625.
https://doi.org/10.1111/j.1751-1097.2011.00912.x

[35] Hanane, B., Jihad, R., Naima, B., *et al.* (2022) Characterisation and Valorisation of the Moroccan Diatomite. *Journal of Geoscience and Environment Protection*, **10**, 109-134. https://doi.org/10.4236/gep.2022.102008

[36] Meyer-Jacob, C., Vogel, H., Boxberg, F., *et al.* (2014) Independent Measurement of Biogenic Silica in Sediments by FTIR Spectroscopy and PLS Regression. *Journal of Paleolimnology*, **52**, 245-255. https://doi.org/10.1007/s10933-014-9791-5

[37] Mcheik, A. (2018) Étude des propriétés photoniques de diatomées. Ph.D. Thesis, Sorbonne Université, Paris.

[38] ALOthman, Z. (2012) A Review: Fundamental Aspects of Silicate Mesoporous Materials. *Materials*, **5**, 2874-2902. https://doi.org/10.3390/ma5122874

[39] De Lange, M.F., Vlugt, T.J.H., Gascon, J., *et al.* (2014) Adsorptive Characterization of Porous Solids: Error Analysis Guides the Way. *Microporous and Mesoporous Materials*, **200**, 199-215. https://doi.org/10.1016/j.micromeso.2014.08.048

[40] Groen, J.C., Peffer, L.A.A. and Pérez-Ramírez, J. (2003) Pore Size Determination in Modified Micro- and Mesoporous Materials. Pitfalls and Limitations in Gas Adsorption Data Analysis. *Microporous and Mesoporous Materials*, **60**, 1-17.
https://doi.org/10.1016/S1387-1811(03)00339-1

[41] Lewin, J.C. (1961) The Dissolution of Silica from Diatom Walls. *Geochimica et Cosmochimica Acta*, **21**, 182-198. https://doi.org/10.1016/S0016-7037(61)80054-9

[42] Iler, R.K. (2004) The Chemistry of Silica: Solubility, Polymerization, Colloid and

Surface Properties, and Biochemistry. Wiley, New York.

[43] Dugger, D.L., Stanton, J.H., Irby, B.N., *et al.* (1964) The Exchange of Twenty Metal Ions with the Weakly Acidic Silanol Group of Silica Gel[1,2]. *The Journal of Physical Chemistry A*, **68**, 757-760. https://doi.org/10.1021/j100786a007

[44] Hurd, D.C. (1973) Interactions of Biogenic Opal, Sediment and Seawater in the Central Equatorial Pacific. *Geochimica et Cosmochimica Acta*, **37**, 2257-2282. https://doi.org/10.1016/0016-7037(73)90103-8

[45] Badaut, D. and Risacher, F. (1983) Authigenic Smectite on Diatom Frustules in Bolivian Saline Lakes. *Geochimica et Cosmochimica Acta*, **47**, 363-375. https://doi.org/10.1016/0016-7037(83)90259-4

[46] Fujii, T., de Groot, F.M.F., Sawatzky, G.A., *et al.* (1999) *In Situ* XPS Analysis of Various Iron Oxide Films Grown by NO_2-Assisted Molecular-Beam Epitaxy. *Physical Review B*, **59**, 3195-3202. https://doi.org/10.1103/PhysRevB.59.3195

[47] van Bommel, M.J. and de Haan, A.B. (1994) Drying of Silica Gels with Supercritical Carbon Dioxide. *Journal of Materials Science*, **29**, 943-948. https://doi.org/10.1007/BF00351414

[48] Uwineza, P.A. and Waśkiewicz, A. (2020) Recent Advances in Supercritical Fluid Extraction of Natural Bioactive Compounds from Natural Plant Materials. *Molecules*, **25**, Article 3847. https://doi.org/10.3390/molecules25173847

[49] Gutmann, V. (1976) Empirical Parameters for Donor and Acceptor Properties of Solvents. *Electrochimica Acta*, **21**, 661-670. https://doi.org/10.1016/0013-4686(76)85034-7

[50] Saint Flour, C. and Papirer, E. (1983) Gas-Solid Chromatography: A Quick Method of Estimating Surface Free Energy Variations Induced by the Treatment of Short Glass Fibers. *Journal of Colloid and Interface Science*, **91**, 69-75. https://doi.org/10.1016/0021-9797(83)90314-4

[51] Van Oss, C.J., Chaudhury, M.K. and Good, R.J. (1988) Interfacial Lifshitz-van der Waals and Polar Interactions in Macroscopic Systems. *Chemical Reviews*, **88**, 927-941. https://doi.org/10.1021/cr00088a006

[52] Gutmann, V. (1978) The Donor-Acceptor Approach to Molecular Interactions. Plenum Press, New York. https://doi.org/10.1007/978-1-4615-8825-2

[53] Laurence, C. and Gal, J.F. (2010) Lewis Basicity and Affinity Scales: Data and Measurement. John Wiley, Chichester. https://doi.org/10.1002/9780470681909

[54] Bauer, F., Meyer, R., Bertmer, M., *et al.* (2021) Silanization of Siliceous Materials, Part 3: Modification of Surface Energy and Acid-Base Properties of Silica Nanoparticles Determined by Inverse Gas Chromatography (IGC). *Colloids and Surfaces A: Physicochemical and Engineering Aspects*, **618**, Article ID: 126472. https://doi.org/10.1016/j.colsurfa.2021.126472

[55] Swann, G.E.A. and Leng, M.J. (2009) A Review of Diatom δ18O in Palaeoceanography. *Quaternary Science Reviews*, **28**, 384-398. https://doi.org/10.1016/j.quascirev.2008.11.002

[56] Zahn, R.K., Zahn-Daimler, G. and Beyer, R. (1988) Highly Protective Alkalinization by Ammonia Vapor Diffusion in Viscosimetric DNA Damage Assessment. *Analytical Biochemistry*, **168**, 387-397. https://doi.org/10.1016/0003-2697(88)90334-X

[57] Shchukarev, A. and Korolkov, D. (2004) XPS Study of Group IA Carbonates. *Open Chemistry*, **2**, 347-362. https://doi.org/10.2478/BF02475578

[58] Mcheik, A., Cassaignon, S., Livage, J., *et al.* (2018) Optical Properties of Nanostructured Silica Structures from Marine Organisms. *Frontiers in Marine Science*, **5**, Ar-

ticle 318703. https://doi.org/10.3389/fmars.2018.00123

[59] Bhardwaj, V. and Mirliss, M.J. (2009) Diatomaceous Earth Filtration for Drinking Water. In: Lehr, J.H. and Keeley, J., Eds., *Water Encyclopedia*, John Wiley & Sons, Hoboken, 2947-2958.

[60] Chen, X., Wang, C., Baker, E. and Sun, C. (2015) Numerical and Experimental Investigation of Light Trapping Effect of Nanostructured Diatom Frustules. *Scientific Reports*, **5**, Article No. 11977. https://doi.org/10.1038/srep11977

[61] Wang, Y., Pan, J., Cai, J., *et al.* (2012) Floating Assembly of Diatom *Coscinodiscus* sp. Microshells. *Biochemical and Biophysical Research Communications*, **420**, 1-5. https://doi.org/10.1016/j.bbrc.2012.02.080

[62] Ye, X. and Qi, L. (2011) Two-Dimensionally Patterned Nanostructures Based on Monolayer Colloidal Crystals: Controllable Fabrication, Assembly, and Applications. *Nano Today*, **6**, 608-631. https://doi.org/10.1016/j.nantod.2011.10.002

[63] Nandi, M., Das, T., Saha, S., *et al.* (2018) Direct Synthesis of Magnesium Doped Mesoporous Silica: Their Catalytic Activity in Knoevenagel Condensation. *Materials Today: Proceedings*, **5**, 10007-10015. https://doi.org/10.1016/j.matpr.2017.10.199

[64] Astrov, Y.A., Shuman, V.B., Portsel, L.M., *et al.* (2017) Diffusion Doping of Silicon with Magnesium. *Physica Status Solidi* (*a*), **214**, Article ID: 1700192. https://doi.org/10.1002/pssa.201700192

[65] Yabu, H., Matsuo, Y., Yamada, T., *et al.* (2020) Highly Porous Magnesium Silicide Honeycombs Prepared by Magnesium Vapor Annealing of Silica-Coated Polymer Honeycomb Films toward Ultralightweight Thermoelectric Materials. *Chemistry of Materials*, **32**, 10176-10183. https://doi.org/10.1021/acs.chemmater.0c03696

[66] Leonardo, S., Prieto-Simón, B. and Campàs, M. (2016) Past, Present and Future of Diatoms in Biosensing. *TrAC Trends in Analytical Chemistry*, **79**, 276-285. https://doi.org/10.1016/j.trac.2015.11.022

[67] Wang, J.K. and Seibert, M. (2017) Prospects for Commercial Production of Diatoms. *Biotechnology for Biofuels*, **10**, Article No. 16. https://doi.org/10.1186/s13068-017-0699-y

[68] Wang, C., Yan, C., Qiu, J., *et al.* (2021) Food Web Biomagnification of the Neurotoxin β-N-Methylamino-L-Alanine in a Diatom-Dominated Marine Ecosystem in China. *Journal of Hazardous Materials*, **404**, Article ID: 124217. https://doi.org/10.1016/j.jhazmat.2020.124217

[69] Van Eynde, E., Lenaerts, B., Tytgat, T., *et al.* (2014) Effect of Pretreatment and Temperature on the Properties of *Pinnularia biosilica* Frustules. *RSC Advances*, **4**, 56200-56206. https://doi.org/10.1039/C4RA09305D

[70] Chetia, L., Kalita, D. and Ahmed, G.A. (2017) Enhanced Photocatalytic Degradation by Diatom Templated Mixed Phase Titania Nanostructure. *Journal of Photochemistry and Photobiology A: Chemistry*, **338**, 134-145. https://doi.org/10.1016/j.jphotochem.2017.01.035

[71] Snelling, A.M., Swann, G.E.A., Leng, M.J., *et al.* (2013) A Micro-Manipulation Technique for the Purification of Diatoms for Isotope and Geochemical Analysis. *Silicon*, **5**, 13-17. https://doi.org/10.1007/s12633-012-9115-1